Experimental investigations of stimulated Raman adiabatic passage in a doped solid

Jens Klein, Fabian Beil,* and Thomas Halfmann†
Institut für Angewandte Physik, Technische Universität Darmstadt, 64289 Darmstadt, Germany
(Received 17 June 2008; published 16 September 2008)

We report on experimental investigations of stimulated Raman adiabatic passage (STIRAP) in a $Pr^{3+}:Y_2SiO_5$ crystal. STIRAP drives complete, coherent population transfer between two hyperfine levels in the Pr^{3+} ions. We investigate the variation of the STIRAP transfer efficiency with the experimental parameters: e.g., detunings, Rabi frequencies, and pulse delays. In addition, we also observe an alternative and efficient, adiabatic transfer process—i.e., *b*-STIRAP—which occurs for a reversed sequence of laser pulses. We compare the efficiencies and time-resolved transfer dynamics of STIRAP and *b*-STIRAP. The experimental data are supported by numerical simulations, also including the effect of laser frequency jitter. Our experimental data and the numerical simulations provide a clear and convincing demonstration of adiabatic excitations in a solid medium.

DOI: 10.1103/PhysRevA.78.033416 PACS number(s): 32.80.Qk, 42.50.Gy

I. INTRODUCTION

The manipulation of atomic and molecular quantum systems, by interaction with coherent radiation fields, exhibits a major research topic in the field of quantum optics. A large variety of coherent techniques serve, e.g., to steer population distributions, to excite atomic coherences, or to control the linear and nonlinear optical response of matter. Adiabatic processes are a subclass of such coherent interactions. The significant advantages of adiabatic interactions are efficiency, selectivity, and robustness with regard to fluctuations in the experimental parameters. Stimulated Raman adiabatic passage (STIRAP) [1] exhibits a prominent example for adiabatic processes. Initially, STIRAP was developed for efficient and selective vibrational excitation of molecules [2]. Meanwhile, STIRAP found a huge number of applications in atomic and molecular physics [3–8]. STIRAP provides complete coherent population transfer in a λ-type quantum system, independent of radiative losses from an intermediate state. STIRAP and its extensions, *fractional* STIRAP and *tripod* STIRAP, are very basic tools for coherent-state manipulation and preparation: e.g., of coherent superpositions [9–14]. Therefore, STIRAP became of great importance for applications in quantum information processing.

Although STIRAP is well established in the gas phase, only a few theoretical proposals suggested implementation in the solid state [15–17]. Very recently, STIRAP was demonstrated in rare-earth-metal-ion-doped dielectric crystals [18–20]. These materials provide excellent properties for the implementation of coherent interactions between light and matter, as they exhibit narrow optical linewidths and long decoherence times. Moreover, due to their large density and scalability, the media are of particular interest for applications in optical data storage and processing. The hyperfine levels of the ground state of the dopant ions are, e.g., well suited for the implementation of qubits. Therefore, such doped solids are considered as promising candidates for quantum information processing [21–24]. However, so far only a few fundamental experimental studies have been conducted [25–29].

In the following, we report on extended and systematic experimental investigations of STIRAP in a $Pr^{3+}:Y_2SiO_5$ crystal (hereafter termed Pr:YSO). The presented data and numerical simulations exhibit a significant extension to our previously published results on STIRAP in Pr:YSO [20]. In these experiments, we observed efficient population transfer for the case of STIRAP as well as for reversed order of the driving laser pulses. The latter case we identified with an alternative adiabatic process, which we termed *b*-STIRAP. In Sec. II we discuss the basics of STIRAP and *b*-STIRAP in detail. In particular, we discuss the effect of laser frequency jitter on both techniques. In Sec. III, we describe the experimental implementation of STIRAP and *b*-STIRAP in Pr:YSO. In Sec. IV we present results from systematic experimental investigations. We investigated the frequency bandwidth of STIRAP and the transfer efficiency with regard to the driving Rabi frequencies and the pulse delays. These results confirm the robustness of STIRAP with respect to variations of experimental parameters. The experimental results show efficient population transfer for STIRAP as well as for *b*-STIRAP. However, only STIRAP permits (almost) complete and fully coherent population transfer. Finally, we also monitored the population dynamics, both for STIRAP and *b*-STIRAP, by time-resolved absorption measurements. Our data are compared to extended numerical simulations of coherent interactions in the doped solid.

II. ADIABATIC PASSAGE PROCESSES IN A THREE-LEVEL SYSTEM

We consider a three-level λ-type quantum system of bare states $|1\rangle$, $|2\rangle$, and $|3\rangle$ (see Fig. 1). Initially, all population is in state $|1\rangle$. The coherent interaction of the quantum system with two laser pulses aims at efficient population transfer to the target state $|3\rangle$. The pump pulse with center frequency ν_P excites the transition between states $|1\rangle$ and $|2\rangle$, with resonance frequency ν_{12}. The Stokes pulse with center frequency ν_S excites the transition between states $|2\rangle$ and $|3\rangle$, with reso-

*Fabian.Beil@physik.tu-darmstadt.de
†URL: http://www.physik.tu-darmstadt.de/nlq

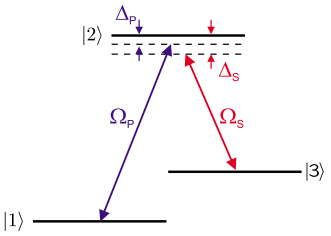

FIG. 1. (Color online) Coupling scheme for STIRAP. A three-level λ-type quantum system interacts with the pump and the Stokes laser pulse. The Rabi frequencies Ω_P and Ω_S describe the coupling strengths of the pump and the Stokes laser field to their corresponding transitions. The detunings from the single-photon resonances are given by Δ_P and Δ_S.

nance frequency ν_{23}. The coupling strengths are defined by the Rabi frequencies $\Omega_P(t)=\mu_{12}\mathcal{E}_P(t)/\hbar$ and $\Omega_S(t)=\mu_{23}\mathcal{E}_S(t)/\hbar$, with the dipole transition moments μ_{ij} and the electric fields of the lasers $\mathcal{E}_{P,S}(t)$.

After a rotating-wave approximation (RWA), the Hamiltonian of the three-level system including the interaction with the laser fields reads in Dirac representation

$$\hat{H}=\frac{\hbar}{2}\begin{pmatrix}0 & \Omega_P(t) & 0\\ \Omega_P^*(t) & -2\Delta_P & \Omega_S^*(t)\\ 0 & \Omega_S(t) & -2(\Delta_P-\Delta_S)\end{pmatrix}, \tag{1}$$

with the detunings Δ_P and Δ_S of the lasers from the corresponding resonances (see Fig. 1). In general, the Rabi frequencies Ω_P and Ω_S are complex quantities. Thus, we write $\Omega_P=|\Omega_P|e^{i\varphi_P}$ and $\Omega_S=|\Omega_S|e^{i\varphi_S}$. Here, φ_P and φ_S are the phases of the two laser fields. For $\Delta_P=\Delta_S=\Delta$, the lasers are tuned to two-photon resonance between states $|1\rangle$ and $|3\rangle$. In this case the instantaneous eigenstates of the system read

$$|b_+\rangle=[(\sin\theta)|1\rangle+e^{i(\varphi_S-\varphi_P)}(\cos\theta)|3\rangle](\sin\phi)+e^{-i\varphi_P}(\cos\phi)|2\rangle,$$

$$|b_-\rangle=[(\sin\theta)|1\rangle+e^{i(\varphi_S-\varphi_P)}(\cos\theta)|3\rangle](\cos\phi)-e^{-i\varphi_P}(\sin\phi)|2\rangle,$$

$$|d\rangle=(\cos\theta)|1\rangle-e^{i(\varphi_S-\varphi_P)}(\sin\theta)|3\rangle. \tag{2}$$

This set of *adiabatic* states includes a *dark* state $|\mathrm{d}\rangle$, which contains no contribution of the optically excited state $|2\rangle$, and the two *bright* states $|b_+\rangle$ and $|b_-\rangle$, which are superpositions of all three bare states. The mixing of the bare states is defined by the two time-dependent angles θ and ϕ given by

$$\theta(t)=\arctan\left(\frac{|\Omega_P(t)|}{|\Omega_S(t)|}\right), \tag{3}$$

$$\phi(t)=\arctan\left(\frac{\sqrt{|\Omega_P(t)|^2+|\Omega_S(t)|^2}}{\sqrt{\Delta^2+|\Omega_P(t)|^2+|\Omega_S(t)|^2}-\Delta}\right). \tag{4}$$

For STIRAP, pump and Stokes laser pulses are applied in a counterintuitive pulse sequence—i.e., the Stokes pulse precedes the pump pulse in a way that the falling edge of the pump pulse is coincident with the rising edge of the Stokes pulse (see Fig. 2). Equations (2) and (3) indicate that, initially (i.e., for $t\to-\infty$), the dark state $|d\rangle$ is equal to the bare state $|1\rangle$. As all the population is initially in this bare state, the quantum system is prepared in the dark state $|d\rangle$. Provided the evolution is adiabatic, the system remains in the dark state during the interaction. At the end of the interaction—i.e., at $t\to+\infty$—we find $|d\rangle\equiv-e^{i(\varphi_S-\varphi_P)}|3\rangle$. Hence, the dark state mediates complete population transfer to the target state. We note that here the phase factor has no relevant physical consequence for the transfer efficiency. As the intermediate state $|2\rangle$ is never populated throughout the interaction, the transfer efficiency is independent of losses from this state. The population dynamics with respect to the bare states is depicted in Fig. 2(a).

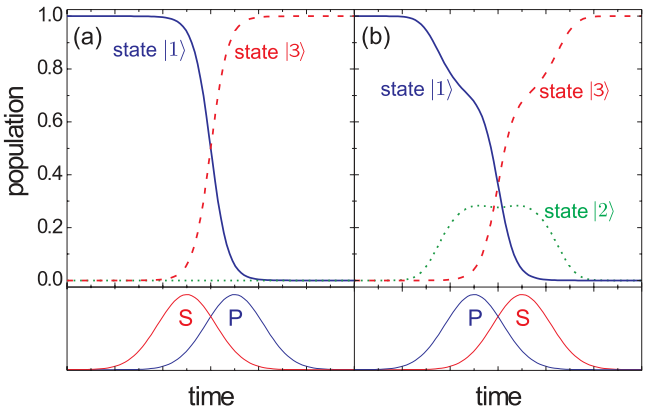

FIG. 2. (Color online) Population transfer by (a) STIRAP and (b) *b*-STIRAP. The corresponding pulse sequences are depicted in the lower part of the diagram.

However, efficient adiabatic population transfer is also possible via one of the bright states, provided certain conditions are fulfilled [20,30]. For this *b*-STIRAP process the driving laser pulses are applied in an intuitive pulse order—i.e., the pump pulse preceding Stokes pulse. Consequently, the projection of the dark state $|d\rangle$ onto the bare state $|1\rangle$ is zero at the beginning of the interaction. The initial state of the system is placed in the subspace of the two bright states. While for $\Delta=0$ the initial state is given as a superposition of the two bright states, the system is prepared in only one of them for $\Delta\neq0$. Consider, e.g., $\Delta>0$. In this case the bright state $|b_+\rangle$ is equal to the initial state $|1\rangle$ before the interaction—i.e., at $t\to-\infty$. For adiabatic evolution the system stays in the bright state $|b_+\rangle$ throughout the interaction. For $t\to+\infty$, this bright state is then equivalent to the target state—i.e., $|b_+\rangle\equiv e^{i(\varphi_S-\varphi_P)}|3\rangle$. Thus, also *b*-STIRAP permits complete adiabatic population transfer. However, as can be seen from the population dynamics depicted in Fig. 2(b), the intermediate state $|2\rangle$ is populated during the interaction process. Thus, *b*-STIRAP is affected by radiative losses from state $|2\rangle$, e.g., to states outside the three-level system. However, for increasing detuning Δ, the amount of transient population in state $|2\rangle$ decreases. Moreover, if the lifetime of the intermediate state is long compared to the duration of the interaction process, the losses are negligible. Thus, for large detuning and/or long lifetime of the intermediate state, effi-

cient population transfer is also possible by interaction with an intuitive pulse sequence—i.e., *b*-STIRAP.

In the above discussion we assumed adiabatic interaction. For perfectly coherent laser pulses, adiabaticity is fully guaranteed by strong coupling—i.e., large Rabi frequencies—and smooth temporal laser profiles. This can be expressed by the adiabaticity condition, which reads [31]

$$||\Delta| - \sqrt{\Delta^2 + |\Omega_P(t)|^2 + |\Omega_S(t)|^2}|\tau \gg 1, \quad (5)$$

where τ is the pulse duration. Under these conditions the state vector of the system follows smoothly the changes of the adiabatic state. Hence, the state vector is fully aligned to a particular adiabatic state (e.g., the dark state in the case of STIRAP) at all times. No diabatic couplings occur. However, in the experiment we must consider laser pulses with limited coherence properties—i.e., frequency jitter. In this case, the laser phases φ_P and φ_S fluctuate in time. Due to the phase factors in Eq. (2), frequency jitter introduces temporal fluctuations in the adiabatic basis. This leads to diabatic couplings.

In our experiment the pump and the Stokes laser pulses are both derived from a single-laser system (see Sec. III) by frequency shifting with acousto-optical modulators. Therefore, the frequency jitters of the two driving laser pulses are equal. The effect of this jitter on STIRAP and *b*-STIRAP is as follows: The dark state $|d\rangle$ depends on the phase difference only—i.e., on $\varphi_P - \varphi_S$. Therefore, STIRAP is not affected by the identical phase fluctuations. In contrast, *b*-STIRAP relies on interaction via the bright states $|b_\pm\rangle$. These states also depend on the phase φ_P of the pump laser alone [see Eq. (2)]. This leads to diabatic coupling between the bright states and to perturbation of the population transfer in *b*-STIRAP.

The sensitivity of STIRAP and *b*-STIRAP with regard to the frequency jitter is illustrated in Fig. 3. In the numerical simulation, the frequency jitter is implemented as statistical changes in laser frequency occurring every 300 ns and exhibiting a Gaussian distribution. The results show that the transfer efficiency of STIRAP is hardly reduced by frequency jitter, even if the jitter bandwidth (FWHM of the Gaussian frequency distribution) approaches the value of the detuning or the Rabi frequencies. In contrast, the transfer efficiency of *b*-STIRAP is strongly affected, even by a modest frequency jitter. The efficiency is reduced to 50%, when the jitter bandwidth approaches the value of the detuning. From theory [31], we know that the difference between the eigenenergies of the adiabatic states is given by the detuning and the Rabi frequencies. These parameters define the relevant range, in which perturbations (e.g., frequency jitter) lead to diabatic couplings and reduced transfer efficiency.

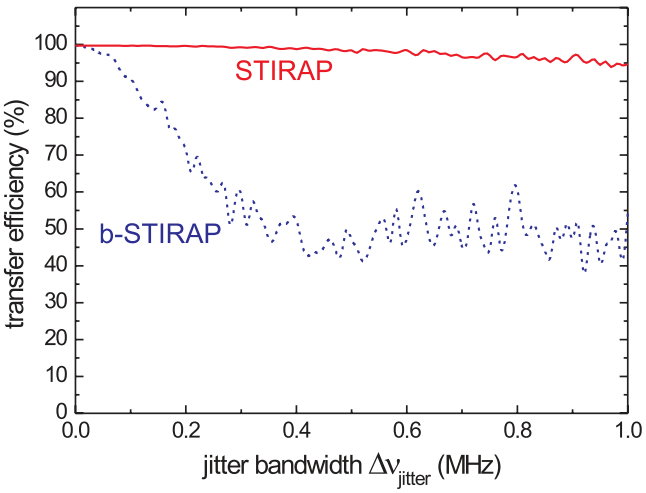

FIG. 3. (Color online) Transfer efficiency vs jitter bandwidth for STIRAP and *b*-STIRAP. The graph shows results from numerical simulations for a three-level quantum system without decay. The laser pulses exhibit a Gaussian temporal shape with a pulse duration $\tau_{P,S}=20$ μs [full width at half maximum (FWHM) of intensity]. Peak Rabi frequencies are $\Omega_P^{(0)}=\Omega_S^{(0)}=2\pi\times 500$ kHz. The detuning from the single-photon resonances is $\Delta=2\pi\times 500$ kHz.

III. EXPERIMENTAL IMPLEMENTATION

A. Coupling scheme in Pr:YSO

In our experiment we implemented STIRAP and *b*-STIRAP in a Pr:YSO crystal. The coupling scheme involves hyperfine components of states $^3H_4$ and $^1D_2$ of the Pr^{3+} ions (see Fig. 4). The hyperfine components are labeled by the magnetic quantum number m_I of the nuclear spin. The pump laser drives the transition between state $|^3H_4, m_I = \pm\frac{1}{2}\rangle \equiv |1\rangle$ and state $|^1D_2, m_I = \pm\frac{3}{2}\rangle \equiv |2\rangle$. The Stokes laser drives the transition between state $|^3H_4, m_I = \pm\frac{3}{2}\rangle \equiv |3\rangle$ and the intermediate state $|2\rangle$. The lifetime of the state $|2\rangle$ is $\tau_2 = 164$ μs[32]. We note that the term "Stokes laser" originates from the first experiments on STIRAP, which aimed at population transfer between vibrational states. In our system, this term refers to the transition between the two initially unpopulated states, rather than to the transition of lower energy.

Due to local variations in the crystal field strength, the optical transition exhibits inhomogeneous broadening. The resulting linewidth exceeds the energy splitting of the hyperfine sublevels by two orders of magnitude. Consequently, a single laser field simultaneously drives different transitions in several ensembles of ions within the inhomogeneous bandwidth. Thus, Pr:YSO exhibits a quite complex spectrum. However, a specific optical preparation sequence based on spectral hole burning [33] allows us to select a single ensemble of praseodymium ions with single, well-defined transition frequencies.

For the preparation sequence, we apply a laser pulse with rectangular temporal shape and a pulse duration of $\tau_{prep} = 84$ ms. The frequency of the laser pulse is initially centered in the inhomogeneous bandwidth at frequency ν_0. The preparation laser frequency ν is repeatedly swept over a range of $0\ \text{MHz} < \nu - \nu_0 < 18\ \text{MHz}$. Ions, which initially exhibit absorption in this spectral range, are optically pumped to other ground-state sublevels. Thus, the absorption in the frequency range of the preparation becomes zero. This broad transmission window within the inhomogeneous bandwidth of the optical transition is called a *spectral pit* [33].

The medium is now ready for interaction with the pump and Stokes pulses. We choose the frequencies of the pump and the Stokes pulse as $\nu_P - \nu_0 = -5$ MHz and $\nu_S - \nu_0 =$

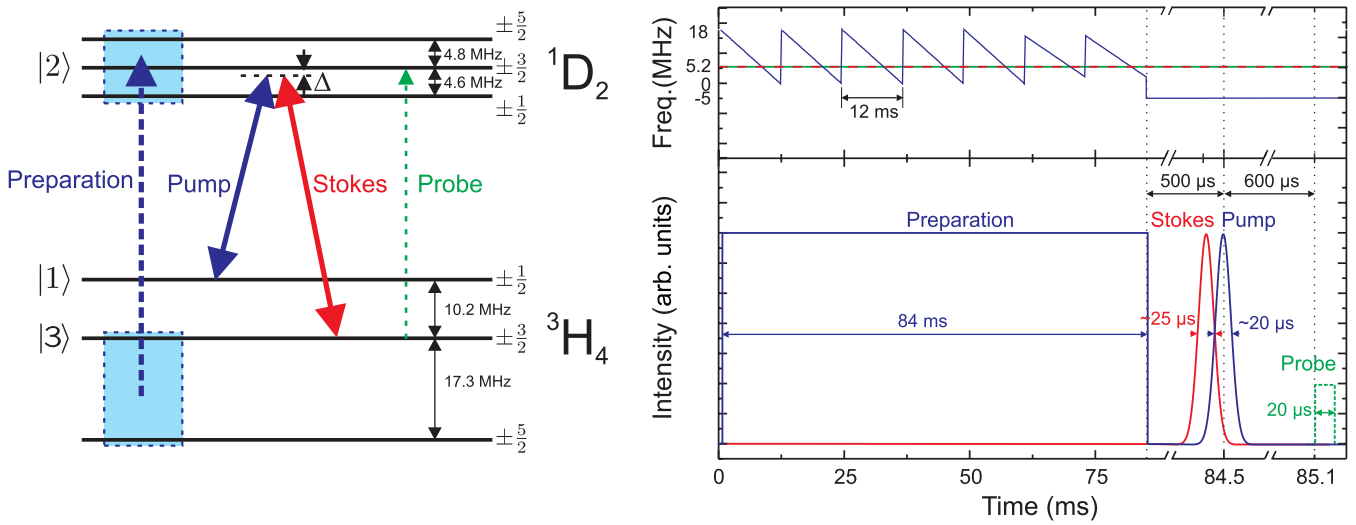

FIG. 4. (Color online) Coupling scheme in Pr:YSO (left) and pulse sequence for preparation, coherent manipulation and probing (right).

+5.2 MHz. The frequency difference between pump and Stokes pulse $\nu_S - \nu_P = +10.2$ MHz is equal to the hyperfine splitting between initial state $|1\rangle$ and target state $|3\rangle$ as depicted in Fig. 4. The pump pulse drives a transition outside the spectral pit; i.e., the pump pulse addresses a state with initial population. The pump pulse experiences absorption. The Stokes pulse drives a transition inside the spectral pit; i.e., the Stokes pulse addresses a state without initial population. The Stokes pulse experiences no absorption. Thus, before the interaction the target state $|3\rangle$ is empty and all the population is in state $|1\rangle$. Therefore, the preparation of the medium and the choice of the pump and Stokes frequencies provides the necessary initial conditions for STIRAP. The pump and Stokes pulse drive population back into the initially empty pit. This leads to absorption at the corresponding transition frequencies within the spectral pit. This absorption is monitored by a well-delayed probe laser pulse and serves as an absolute measure for the population transfer efficiency.

We choose the probe laser frequency close to the Stokes laser frequency. Consequently, the population of the target state is monitored by absorption on the transition $|3\rangle \rightarrow |2\rangle$. The frequency difference between Stokes and probe laser $\nu_S - \nu_{pr}$ corresponds to the detuning of pump and Stokes laser from the single-photon resonances. The choice of the probe transition provides the selectivity of the implemented coupling scheme. As the pump frequency is outside the spectral pit, the pump pulse is not selective to a specific ensemble of Pr^{3+} ions, but drives different transitions simultaneously in nine ensembles. However, the probe laser monitors a change in absorption only in three ensembles, in which the pump and the probe laser address transitions between the hyperfine levels of the ground state with $m_I = \pm\frac{1}{2}$ and $m_I = \pm\frac{3}{2}$, respectively, and the same excited state sublevel. The coupling schemes in these three ensembles are depicted in Fig. 5. From these three ensembles only ions of type II ("STIRAP ensemble") are relevant for STIRAP. For the ions of type I the oscillator strength of the Stokes and probe transition is very low. This leads to some negligible background in the probe laser absorption by an ineffective Raman coupling. The maximum background is less than 2% of the total absorption. Moreover, we experimentally verified by additional absorption measurements that the ionic ensemble of type III does not play any role, as the initial state $|1\rangle$ in this ensemble is totally emptied by the preparation process. Consequently, only the ionic ensemble of type II is relevant for the calibration of the population transfer efficiency. In the experiment, we monitor the change in probe absorption, when the STIRAP laser pulses are switched either on or off. From Beer's law we get

$$\Delta\alpha = -\frac{1}{l}\ln\frac{T'}{T}, \tag{6}$$

with the transmission T' and T with and without the STIRAP pulses, and the length of the medium l. As we only consider ions of type II, the change in the absorption can be directly related to the relative population P_3 in the target state after the population transfer process. The relation reads

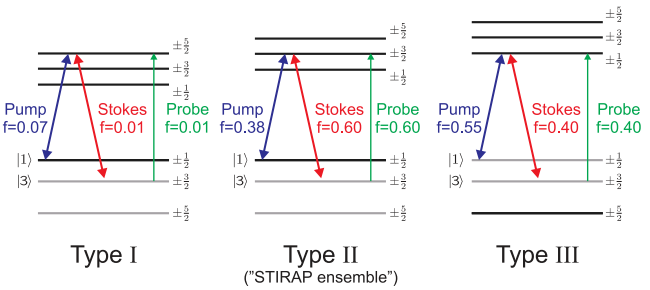

FIG. 5. (Color online) Selectivity of population transfer and probing. In principle, the pump and Stokes laser can drive population transfer in three different ionic ensembles. The figure shows the relevant coupling schemes and oscillator strength in these ensembles [33]. For the calibration of the transfer efficiency by STIRAP, we must consider only ions of type II. Due to appropriate preparation or low oscillator strength, the other ensembles do not matter in the experiment (see text).

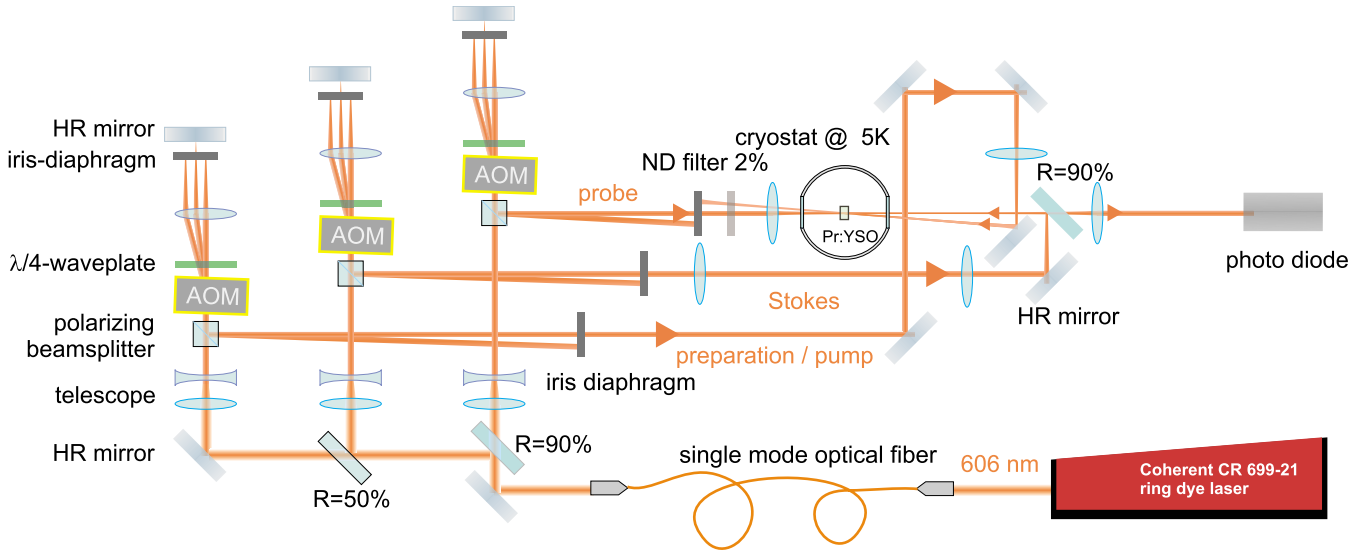

FIG. 6. (Color online) Experimental setup.

$$\Delta\alpha = \alpha_0 f_{pr} P_3, \tag{7}$$

with the absorption coefficient α_0 in the thermal equilibrium and the relative oscillator strength f_{pr} of the probe transition. For our Pr:YSO sample (dopant concentration 0.02%), we experimentally determined $\alpha_0 = 12.3\ \mathrm{cm}^{-1}$. We assume that initially all ions of the relevant ensemble are in state $|1\rangle$—i.e., $P_1 = 1$ and $P_3 = 0$. Thus, after the interaction P_3 is equivalent to the population transfer efficiency. Therefore, the transfer efficiency is calibrated from Eq. (7), using the oscillator strength $f_{pr} = 0.60$ [33]. We confirmed experimentally, that the underlying assumptions are well justified.

B. Experimental setup

In the experiments, we apply a Pr:YSO crystal (length $l = 3$ mm) with a dopant concentration of 0.02%. The crystal is cooled to cryogenic temperatures of less than 5 K in a closed-cycle cryostat (Janis SHI-4-1-331S). A single-longitudinal-mode dye laser (Coherent 699) provides radiation at $\lambda = 605.98$ nm to drive the relevant transition in the Pr^{3+} ions. The laser linewidth is determined by frequency jitter. On long time scales—i.e., exceeding 1 ms—the jitter bandwidth is approximately 1 MHz. On a time scale of a few 10 μs (i.e., as relevant for our experiment), we deduced a jitter bandwidth of up to 250 kHz.

The laser radiation is split into three beamlines (see Fig. 6). Acousto-optical modulators (AOMs) in double-pass configuration serve to modulate the intensity and shift the frequency of the laser radiation in each beam independently. Thus, the preparation, pump, Stokes, and probe laser pulses are all derived from a single laser source. Consequently, the frequency jitter of the source leads to identical phase fluctuations in all laser pulses.

The control signals for intensity modulation and frequency control are provided by arbitrary wave-form generators (Agilent 33220A). The resulting temporal shapes of the pump and the Stokes pulse are slightly different from an ideal Gaussian temporal profile (see Fig. 10). This is due to the nonlinear response of the radio frequency drivers of the AOMs. However, the temporal pulse profiles are still smooth and therefore suitable to drive adiabatic processes. The pulse envelopes are close to a Gaussian shape with durations (FWHM of intensity) of $\tau_P = 19.8$ μs for the pump pulse and $\tau_S = 24.6$ μs for the Stokes pulse. The pump pulse is delayed by 500 μs with respect to the end of the preparation pulse sequence. The delay between the pump and Stokes pulse was systematically varied in the experiment. The probe pulse exhibits a rectangular temporal profile with a pulse duration of $\tau_{pr} = 20$ μs. The probe pulse is delayed by 600 μs with respect to the pump pulse. This allows for decay of residual population in the excited state after the excitation process and to directly relate the probe laser absorption to the population of the target state.

The laser pulses are linearly polarized and overlap in the Pr:YSO sample. In the crystal, the diameters (FWHM of intensity) of the preparation, pump, and Stokes beam are approximately $d_{P,S} = 295$ μm. The diameter of the probe beam is $d_{pr} = 175$ μm. Therefore, the probe laser monitors ions in the intense centers of the pump and Stokes laser beam. The laser powers are approximately $P_P = 100$ mW for the preparation and pump beam, $P_S = 65$ mW for the Stokes beam, and $P_{pr} = 12$ μW for the probe beam. The resulting intensities in the interaction region correspond to peak Rabi frequencies $\Omega_P^{(0)} = 2\pi \times 703$ kHz, $\Omega_S^{(0)} = 2\pi \times 715$ kHz, and $\Omega_{pr}^{(0)} = 2\pi \times 14$ kHz. The weak probe is counterpropagating with respect to the other beams, which are overlapped under a small angle. After passing the sample, a part of the probe laser intensity is directed onto a silicon photodiode to determine the transmission of the sample.

IV. EXPERIMENTAL RESULTS

A. Transfer efficiency vs single-photon detuning

In a first experiment, we recorded absorption spectra by variation of the probe lasers frequency. The pump and Stokes lasers are tuned to the corresponding resonances. The delay

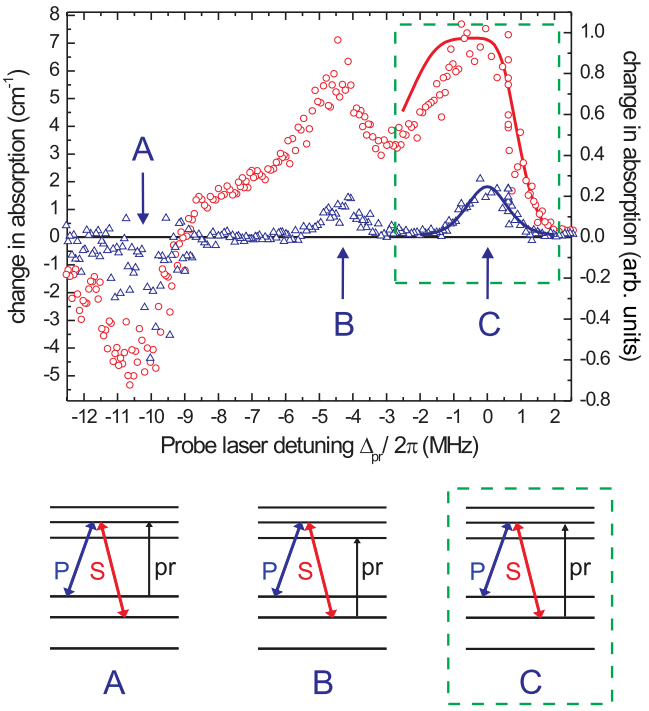

FIG. 7. (Color online) Changes in the absorption spectrum induced by optical pumping [(blue) triangles] and STIRAP [(red) circles]. The probe laser frequency is given relative to the frequency of the Stokes laser. The absorption features *A*, *B*, and *C* are explained by the corresponding coupling schemes below. The absorption feature *C* corresponds to the relevant probe transition. The solid lines are results from numerical simulations.

of the Stokes pulse with respect to the pump pulse is $\Delta t = -15\ \mu$s; i.e., the Stokes pulse precedes the pump pulse. Figure 7 shows the change in absorption versus the detuning of the probe laser from the relevant transition $|3\rangle \rightarrow |2\rangle$. We compare experimental data for the case of optical pumping, i.e., when only the pump laser is switched on [see Fig. 7 (blue) triangles] and for the case of STIRAP, i.e., when pump and Stokes are switched on [see Fig. 7 (red) circles].

In the case of optical pumping, a fraction of the resonantly excited ions is driven to the intermediate state $|2\rangle$ by the pump laser. Spontaneous decay leads to a population of the target state $|3\rangle$. This results in an increase in absorption at the probe transition at resonance—i.e., at a detuning of $\Delta_{pr}/2\pi = 0$ MHz [see Fig. 7 (blue) triangles, position *C*]. This feature in the absorption spectrum is relevant for the calibration of the transfer efficiency by STIRAP, as discussed below. However, we also observe some other features in the spectrum. At a probe laser detuning $\Delta_{pr}/2\pi = -4.6$ MHz (position *B*) we observe another peak in the absorption. Here the probe laser frequency is resonant with the transition between the target state $|3\rangle$ and the excited state $|^1D_2, m_I = \pm\frac{1}{2}\rangle$ (see coupling schemes in lower part of Fig. 7). At a probe laser detuning $\Delta_{pr}/2\pi = -10.2$ MHz (position *A*), we observe a negative feature. Here, the probe laser is resonant with the pump transition. Thus, the reduced population of the initial state $|1\rangle$ leads to a reduced absorption of the probe laser.

In the case of STIRAP [see Fig. 7 (red) circles] the modulation of the absorption spectrum is significantly larger than in the case of optical pumping. Already this fact indicates the large efficiency of the adiabatic process. When the probe laser is tuned to the relevant resonance (i.e., at $\Delta_{pr}/2\pi = 0$ MHz), the maximum absorption is a factor of 4 larger than in the case of optical pumping. The absolute value of this maximum absorption (see left axis) corresponds to a population transfer efficiency near unity. We normalized the scale of the right axis accordingly. Note that this scale in terms of transfer efficiency applies only to the absorption feature *C*. The other absorption lines involve transitions with different oscillator strengths.

The spectral line *C* shows an increased width and an asymmetry. As the pump laser frequency is outside the spectral pit, the pump interacts with a broad distribution of ensembles. These ensembles are all prepared in the same ground-state sublevel, but they exhibit different resonance frequencies for the transition $|2\rangle \rightarrow |1\rangle$. Thus, STIRAP simultaneously drives several ensembles with different detunings of the pump and Stokes lasers from the single-photon resonances. When we tune the probe laser, we monitor population transfer in some selected of these ensembles. However, due to the low probe intensity, the absorption measurement is limited to a subset of ensembles, with resonance frequencies within the linewidth of the probe laser pulse. Thus, the probe laser detuning in Fig. 7 corresponds to the negative value of the single-photon detuning of pump and Stokes laser in the specific ensemble of ions, which is addressed by the probe laser. Thus, the width of the absorption line indicates the broad range of single-photon detunings, which permit efficient transfer by STIRAP. As typical for an adiabatic process, the transfer efficiency does not rely on the exact choice of the experimental parameters: e.g., the single-photon detuning.

We note that the asymmetry of the absorption line cannot be explained by the simple model of a three-level quantum system, discussed in Sec. II. Thus, we considered in our simulation the full six-level scheme of Pr:YSO, and the couplings of the pump and Stokes lasers on all nine possible transitions. This extended model reproduces the line shape in the relevant spectral range quite well (see Fig. 7).

In terms of an analytical explanation, the asymmetry of the line shape is based on quantum interference between the two Raman excitation pathways involving the excited-state sublevels $|^1D_2, m_I = \pm\frac{1}{2}\rangle$ and $|^1D_2, m_I = \pm\frac{3}{2}\rangle$. If the pump and Stokes laser fields are tuned in between the intermediate states of the two λ systems, population transfer is suppressed by destructive quantum interference. This results in the asymmetric line shape. We note that the coupling via the excited-state sublevel $|^1D_2, m_I = \pm\frac{5}{2}\rangle$ is negligible, due to low oscillator strength.

B. Transfer efficiency vs Rabi frequency

We studied the dependence of the transfer efficiency by STIRAP with respect to the peak Rabi frequencies of the pump and the Stokes laser (see Fig. 8). The probe laser frequency was tuned to the center of the relevant absorption line (see Fig. 7, position *C*) in the case of STIRAP. This corresponds to a probe detuning $\Delta_{pr} \approx -2\pi \times 400$ kHz. In the

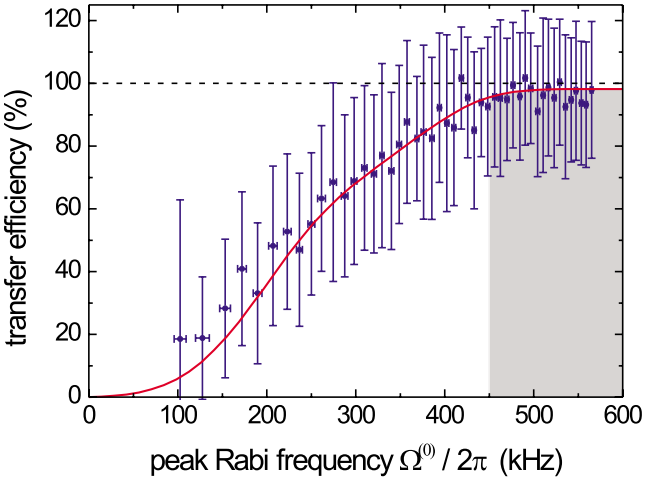

FIG. 8. (Color online) Transfer efficiency of STIRAP vs peak Rabi frequency. The intensities of pump and Stokes laser fields are varied simultaneously such that $\Omega_P^{(0)} \approx \Omega_S^{(0)}$. Experimental data [(blue) squares] and numerical simulation [(red) line].

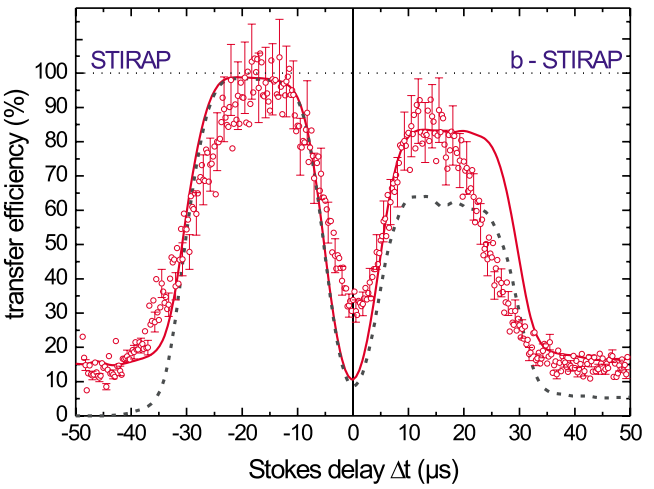

FIG. 9. (Color online) Transfer efficiency vs delay of the Stokes pulse with respect to the pump pulse. Experimental data [(red) circles] show efficient population transfer for delayed laser pulses. A full numerical simulation (solid line) includes frequency jitter and additional off-resonant couplings in the six-level system of Pr:YSO. In a reduced numerical simulation (dashed line), we excluded the decay to the target state $|3\rangle$.

experiment, we varied the laser intensities of the pump and Stokes pulses in parallel. Consequently, the peak Rabi frequencies were equal throughout the measurement—i.e., $\Omega_P^{(0)} \approx \Omega_S^{(0)}$.

Due to the additional losses in the slightly extended optical setup for this particular experiment, the maximum peak Rabi frequencies are considerably lower than in our other experiments. Anyway, also for this reduced range of intensities, the transfer efficiency exhibits a plateau approaching 100% for Rabi frequencies exceeding $\Omega_{P,S}^{(0)} \approx 2\pi \times 450$ kHz (indicated by the shaded area in Fig. 8). The experimental data agree well with numerical simulations. The data indicate the efficiency and the robustness of STIRAP, also with regard to variations in the Rabi frequencies, provided we exceed the threshold for adiabatic evolution. For lower Rabi frequencies, the transfer efficiency decreases with decreasing Rabi frequency, as expected. The threshold for adiabatic evolution in our experiment is determined by the common single-photon detuning $\Delta = -\Delta_{pr} \approx 2\pi \times 400$ kHz. This can be seen from Eq. (5). If the Rabi frequencies Ω_P and Ω_S fall below the detuning Δ, the left-hand side of Eq. (5) becomes small and, therefore, the adiabaticity condition is not fulfilled.

C. Transfer efficiency vs pulse delay

We monitored the variation of the transfer efficiency versus the delay of the Stokes pulse with respect to the pump pulse. The peak Rabi frequencies were $\Omega_{P,S}^{(0)} \approx 2\pi \times 700$ kHz. Figure 9 shows the experimental results. Negative values of the Stokes delay correspond to a counter intuitive pulse sequence; i.e., the Stokes pulse precedes the pump pulse (STIRAP). Positive Stokes delays correspond to an intuitive pulse sequence; i.e., the pump pulse precedes the Stokes pulse (*b*-STIRAP).

Both for positive and negative delay, we observe plateaus of efficient population transfer. These plateaus clearly indicate robust, adiabatic population transfer—i.e., the exact delay is of minor importance—as long as adiabaticity is maintained. The maximum transfer efficiencies in both cases exceed the transfer efficiency for coincident laser pulses by almost a factor of 3. For incoherent interaction the maximum transfer efficiency would be expected at zero delay. In contrast, for coherent interaction, efficient transfer is expected at delays in the order of the pulse durations (i.e., around 20 μs), when the edges of both pulses overlap in time. Such delays provide the required time evolution of the Rabi frequencies for STIRAP (negative delay) or *b*-STIRAP (positive delay) as discussed in Sec. II. Thus, efficient transfer for delayed laser pulses is already clear evidence for coherent interaction. In the case of STIRAP the transfer efficiency approaches unity. In the case of *b*-STIRAP the maximum transfer efficiency is slightly reduced. This is due to residual incoherent losses from the intermediate state $|2\rangle$ and diabatic couplings, induced by the frequency jitter of the laser pulses. As already discussed above, *b*-STIRAP is much more sensitive to frequency jitter than STIRAP.

Compared to our previous publication on the subject [20], we extended our numerical simulation. The simulation includes now the frequency jitter during the interaction time, as well as additional couplings outside an ideal three-level quantum system. The full numerical simulation agrees well with the experimental data. The most pronounced discrepancy between simulation and measurement is seen at positive Stokes delays exceeding $\Delta t = 20$ μs. Thus, the pulses exhibit an intuitive order and only little temporal overlap. Consequently, the adiabaticity is weak and the transfer efficiency strongly depends on the experimental parameters. In this case, a discrepancy between experiment and numerical simulation is most likely. We also performed a reduced numerical simulation, which excluded the decay to the target state $|3\rangle$ (see Fig. 9, dashed line). Comparison of the full and reduced numerical simulations shows that the population transfer is

fully coherent in the case of STIRAP, while *b*-STIRAP also contains an incoherent contribution. Again, the complete population transfer by STIRAP, also in the presence of a frequency jitter, demonstrates the advantages of STIRAP. Nevertheless, also *b*-STIRAP exhibits an alternative and efficient transfer process. *b*-STIRAP permits large transfer efficiency in our coupling scheme, because the lifetime of the intermediate state $|2\rangle$ is longer than the pulse durations—i.e., the interaction time. However, *b*-STIRAP suffers more from frequency jitter than STIRAP. This leads to a diabatic coupling between the bright states and a residual population in the intermediate state $|2\rangle$. A fraction of this residual population decays to the target state $|3\rangle$ and gives rise to an incoherent contribution to the overall transfer efficiency.

D. Time-resolved population dynamics

We also monitored the *time-resolved* population dynamics of STIRAP and *b*-STIRAP. Thus, we varied the delay of the probe laser pulse with respect to the pump and Stokes laser pulses. For appropriate temporal resolution, we set the probe pulse duration to $\tau_{pr}=5$ μs. Now the probe process is no longer temporally separated from the coherent population transfer process. Therefore we must consider the effect of population P_2 in the intermediate state $|2\rangle$ during the probing process. The measured absorption coefficient is now proportional to the population difference P_3-P_2, rather than simply to P_3.

In addition to our previous results on the subject [20], we also investigated the population dynamics for *b*-STIRAP and for optical pumping. For *b*-STIRAP the delay of the Stokes pulse with respect to the pump pulse is $\Delta t=+14$ μs, while for STIRAP we have $\Delta t=-15$ μs.

Figure 10 shows the time-resolved population dynamics. For the case of optical pumping we observe a negative population difference when the medium interacts with the pump laser pulse. At this time, the resonant ions are excited to the intermediate state $|2\rangle$. Thus, the medium is driven to population inversion on the probe transition, because initially the target state $|3\rangle$ is empty. As the excited-state population decays by spontaneous emission, the population inversion is reduced. More and more ions decay to the target state $|3\rangle$, until the population difference asymptotically approaches 13% for late times.

In the case of STIRAP [see Fig. 10(b)] the population dynamics changes significantly. During the interaction with the pump and Stokes pulse, we observe a rapid increase of the population difference to 100%—i.e., a nearly complete population transfer to the target state $|3\rangle$. The population difference is positive for all times. This indicates that the intermediate state $|2\rangle$ is never significantly populated during the STIRAP process. The observed evolution of the target-state population agrees very well with an analytical theoretical prediction (solid line). The calculation is based on the expressions for the adiabatic eigenstates and the mixing angles [see Eqs. (2) and (3)].

Also for *b*-STIRAP, we observe efficient population transfer to the target state $|3\rangle$ during the interaction with pump and Stokes pulse. However, now the population difference also yields negative values in the beginning of the interaction. In *b*-STIRAP, the medium interacts first with the pump pulse. As in the case of optical pumping this leads initially to population inversion on the probe-Stokes transition. However, when the Stokes intensity increases, the population difference changes quickly to positive values. The target state $|3\rangle$ becomes populated by adiabatic passage. At the end of the interaction also some excited-state population flows adiabatically to the target state. Thus, the population difference is further increased. A theoretical prediction deviates somewhat from the experimental data. The simple analytical model does not include spontaneous decay during the interaction, as well as diabatic couplings due to frequency jitter. However, there is still a good qualitative agreement between the experimental data and the pretty simple theoretical prediction.

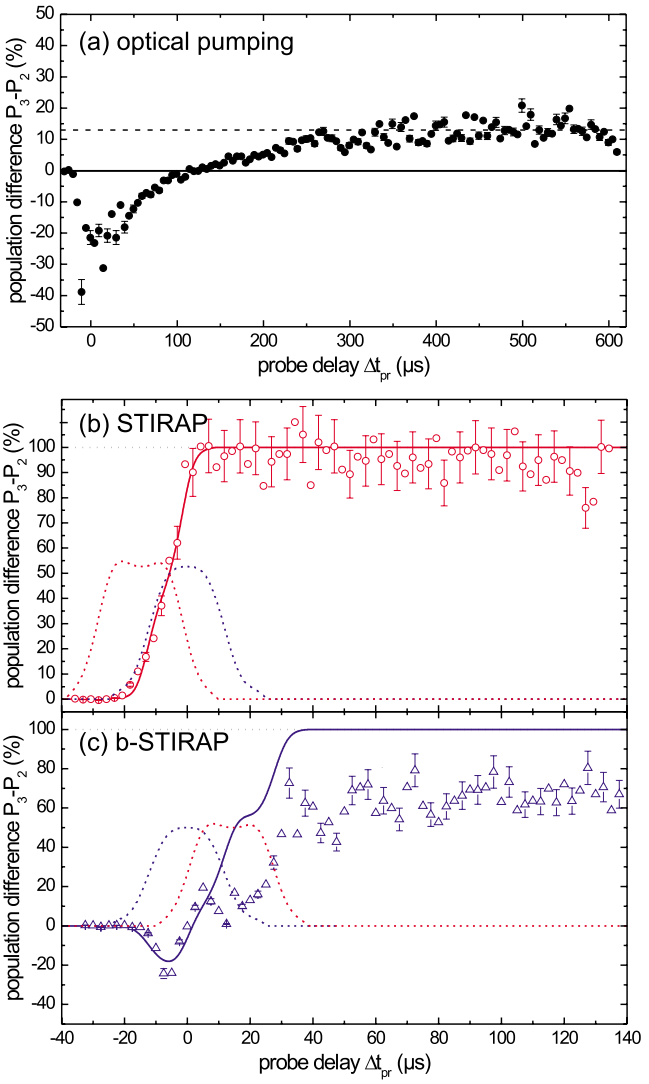

FIG. 10. (Color online) Population dynamics of (a) optical pumping, (b) STIRAP, and (c) *b*-STIRAP. The probe delay is measured relative to the peak of the pump pulse. The figures also indicate the temporal profiles of the pump (dashed line) and Stokes (dotted line) Rabi frequencies. Solid lines show analytical theoretical predictions.

V. CONCLUSION

We performed systematic experimental investigations on coherent, adiabatic population transfer between hyperfine states of Pr^{3+} ions doped in a Y_2SiO_5 host crystal. The dopant ions are driven by two laser pulses—i.e., the pump and the Stokes pulse. We observed robust and complete population transfer by STIRAP—i.e., in a counterintuitive sequence of the driving laser pulses. We also monitored efficient population transfer driven by an intuitive pulse sequence. This is due to an alternative adiabatic transfer process, which we termed *b*-STIRAP. The transfer efficiency exceeded the limits, expected from considerations of incoherent excitations, by far. The experimental data, as well as the theoretical and numerical analysis, indicate that *b*-STIRAP is less robust than STIRAP. In contrast to STIRAP, *b*-STIRAP is much more affected by radiative losses from an intermediate state as well as by frequency jitter. Still, if the time scale of the interaction is considerably smaller than the relevant radiative lifetime of the medium and the frequency jitter does not exceed the relevant detunings and driving Rabi frequencies, *b*-STIRAP provides an interesting alternative for adiabatic population transfer in a three-level system.

In our systematic experimental investigations we monitored the transfer efficiency versus the single-photon detuning, the Rabi frequencies, and the Stokes delay. We provided absolute calibration of the transfer efficiency by measurements of absorption. The data revealed the efficiency and robustness of adiabatic passage processes with regard to the experimental parameters—provided some limits are kept in view. We compared the experimental results with numerical simulations, including the full six-level scheme of Pr:YSO and laser frequency jitter. The data agree well with the extended simulations. Moreover, we monitored the time-resolved population dynamics of STIRAP and *b*-STIRAP. We compared the temporal evolution of the adiabatic processes to optical pumping, as well as to theoretical predictions. Our investigations clearly reveal the possibilities of coherent, adiabatic interactions in the environment of a solid.

ACKNOWLEDGMENTS

The authors thank B. W. Shore (Livermore, CA, USA), K. Bergmann (University of Kaiserslautern), M. Oberst (University of Kaiserslautern), and F. Vewinger (University of Bonn) for most valuable discussions. We acknowledge funding by the Deutsche Forschungsgemeinschaft and the European Union.

[1] N. V. Vitanov, T. Halfmann, B. W. Shore, and K. Bergmann, Annu. Rev. Phys. Chem. **52**, 763 (2001).
[2] U. Gaubatz, P. Rudecki, S. Schiemann, and K. Bergmann, J. Chem. Phys. **92**, 5363 (1990).
[3] H. G. Rubahn, E. Konz, S. Schiemann, and K. Bergmann, Z. Phys. D: At., Mol. Clusters **22**, 401 (1991).
[4] H. Theuer and K. Bergmann, Eur. Phys. J. D **2**, 279 (1998).
[5] M. Hennrich, T. Legero, A. Kuhn, and G. Rempe, Phys. Rev. Lett. **85**, 4872 (2000).
[6] V. Kurkal and S. A. Rice, Chem. Phys. Lett. **344**, 125 (2001).
[7] T. Cubel, B. K. Teo, V. S. Malinovsky, J. R. Guest, A. Reinhard, B. Knuffman, P. R. Berman, and G. Raithel, Phys. Rev. A **72**, 023405 (2005).
[8] K. Winkler, F. Lang, G. Thalhammer, P. v. d. Straten, R. Grimm, and J. H. Denschlag, Phys. Rev. Lett. **98**, 043201 (2007).
[9] N. V. Vitanov, K.-A. Suominen, and B. W. Shore, J. Phys. B **32**, 4535 (1999).
[10] R. Unanyan, M. Fleischhauer, B. W. Shore, and K. Bergmann, Opt. Commun. **155**, 144 (1998).
[11] L. M. Duan, J. I. Cirac, and P. Zoller, Science **292**, 1695 (2001).
[12] F. Vewinger, M. Heinz, R. Garcia Fernandez, N. V. Vitanov, and K. Bergmann, Phys. Rev. Lett. **91**, 213001 (2003).
[13] F. Vewinger, M. Heinz, B. W. Shore, and K. Bergmann, Phys. Rev. A **75**, 043406 (2007).
[14] F. Vewinger, M. Heinz, U. Schneider, C. Barthel, and K. Bergmann, Phys. Rev. A **75**, 043407 (2007).
[15] U. Hohenester, F. Troiani, E. Molinari, G. Panzarini, and C. Macchiavello, Appl. Phys. Lett. **77**, 1864 (2000).
[16] U. Hohenester, J. Fabian, and F. Troiani, Opt. Commun. **264**, 426 (2006).
[17] J. Siewert, T. Brandes, and G. Falci, Opt. Commun. **264**, 435 (2006).
[18] H. Goto and K. Ichimura, Phys. Rev. A **74**, 053410 (2006).
[19] H. Goto and K. Ichimura, Phys. Rev. A **75**, 033404 (2007).
[20] J. Klein, F. Beil, and T. Halfmann, Phys. Rev. Lett. **99**, 113003 (2007).
[21] K. Ichimura, Opt. Commun. **196**, 119 (2001).
[22] N. Ohlsson, R. K. Mohan, and S. Kröll, Opt. Commun. **201**, 71 (2002).
[23] J. Wesenberg and K. Mølmer, Phys. Rev. A **68**, 012320 (2003).
[24] J. H. Wesenberg, K. Mølmer, L. Rippe, and S. Kröll, Phys. Rev. A **75**, 012304 (2007).
[25] M. Nilsson, L. Levin, N. Ohlsson, T. Christiansson, and S. Kröll, Phys. Scr. **T102**, 178 (2002).
[26] J. J. Longdell and M. J. Sellars, Phys. Rev. A **69**, 032307 (2004).
[27] J. J. Longdell, M. J. Sellars, and N. B. Manson, Phys. Rev. Lett. **93**, 130503 (2004).
[28] L. Rippe, M. Nilsson, S. Kröll, R. Klieber, and D. Suter, Phys. Rev. A **71**, 062328 (2005).
[29] L. Rippe, B. Julsgaard, A. Walther, Y. Ying, and S. Kroll, Phys. Rev. A **77**, 022307 (2008).
[30] N. V. Vitanov and S. Stenholm, Opt. Commun. **135**, 394 (1997).
[31] N. Vitanov, B. Shore, L. Yatsenko, K. Böhmer, T. Halfmann, T. Rickes, and K. Bergmann, Opt. Commun. **199**, 117 (2001).
[32] R. W. Equall, R. L. Cone, and R. M. Macfarlane, Phys. Rev. B **52**, 3963 (1995).
[33] M. Nilsson, L. Rippe, S. Kröll, R. Klieber, and D. Suter, Phys. Rev. B **70**, 214116 (2004).